MRS Advances © The Author(s), 2020, published on behalf of Materials Research Society by Cambridge University Press
DOI: 10.1557/adv.2020.371

Study of the performance of $Sn_xSb_yS_z$/carbon nanofibers composite as anode of sodium-ion batteries

L.A. Rodríguez-Guadarrama[1], J. Escorcia-García[2], E. Quiroga-González[3], I.L. Alonso-Lemus[4,*]

[1] *CINVESTAV, Unidad Saltillo, Sustentabilidad de los Recursos Naturales y Energía, Av. Industria Metalúrgica 1062, Parque Industrial, Ramos Arizpe 25900, Coahuila, Mexico.*

[2] *CONACYT-CINVESTAV, Unidad Saltillo, Av. Industria Metalúrgica 1062, Parque Industrial, Ramos Arizpe 25900, Coahuila, México.*

[3]*Institute of Physics, Benemérita Universidad Autónoma de Puebla, San Claudio and 184 Sur 72574, Puebla, Mexico.*

[4]*CONACYT-CINVESTAV, Unidad Saltillo, Sustentabilidad de los Recursos Naturales y Energía, Av. Industria Metalúrgica 1062, Parque Industrial, Ramos Arizpe 25900, Coahuila, México.*

* Email: I.L. Alonso-Lemus (ivalemus@gmail.com)

Sodium-ion batteries (SIBs) have emerged as a promising alternative for energy storage. In this work, it has been synthesized a nanocomposite material of $Sb_xSb_yS_z$*/Carbon nanofibers (CNFs) using low-cost synthesizing methods. First, CNFs have been obtained by electrospinning method with subsequent carbonation at 700°C. Afterward, a* $Sb_xSb_yS_z$ *thin coating is deposited on the CNFs by chemical bath deposition technique to obtain the* $Sb_xSb_yS_z$*/CNFs. In order to obtain the* $SnSb_2S_4$ *crystalline phase, the composite is heated at 300°C in nitrogen atmosphere. The evaluation of this nanocomposite as the anode for SIBs has a reversible discharge capacity of 180 mAh* g^{-1} *and a columbic efficiency of*

61.4% after 9 cycles. On the other hand, the resistance associated to the charge transfer to the CNFs decreases from 115.03 Ω to 77.86 Ω due to the incorporation of $Sn_xSb_yS_z$. Finally, an easy and inexpensive route has been proposed for the synthesis of $Sb_xSb_yS_z$/CNFs composite with great potential to be used as anode material for SIBs.

1. INTRODUCTION

In recent years, sodium-ion batteries (SIBs) have been studied as candidates to replace lithium-ion batteries (LIBs) in portable electronic devices, electric vehicles, and large-scale energy storage, due to the high-abundance of sodium and the similarity of its electrochemical properties mainly to lithium. In this regard, the Na^+ and Li^+ intercalation processes are very similar for cathode materials [1,2]. Therefore, there has been significant progress in the development of these materials for SIBs cathodes [3,4,5].

However, anode materials are a challenge in SIBs. The most studied materials for this purpose are based on carbon (e.g. nanowires, nanofibers, nanobelts, nanorods, and nanotubes) [6,7], showing promising performances. However, other materials have been also tested. Of particular interest are the ones based on Sn and Sb, due to their low price, low-toxicity, and abundance. Among these materials ones find SnS, SnO_2, Sb_2Sb_3, Sb_2O_3, $Sn_xSb_yS_z$) [8,9]. However, the best results have been obtained when they are in the form of composite with carbonaceous materials like carbon nanofibers (CNF), as is the case of SnS/CNF and Sb_2S_3/CNF [10-11]. Another finding has been that when the chalcogenide is ternary with Sn and Sb ($SnSbS_x$/PCNFs), the performance has been surprising, with a reversible capacity of 566.7 mAh g^{-1} after 80 cycles and a current density of 100 mA g^{-1} [12]. However, it is not known if the relatively high capacity comes from the structure of the compound, or from the composition.

In this work, anodes of a solution of SnS, Sb_2S_3 and $SnSb_2S_4$ (overall composition $Sn_xSb_yS_z$) forming a composite with CNFs are evaluate of the enhancement of capacity reported in [12] is given by the structure of ternary chalcogenide (in the present case one does not deal with a single structure). The composite has been synthesized by combining the electrospinning and chemical bath deposition (CBD) techniques, which are simple, cheap, and low energy consumption methods. The morphological, structural, and chemical properties as well as the electrochemical performance have been examined.

2. EXPERIMENTAL SECTION

2.1 Preparation of $Sn_xSb_yS_z$/CNF composite

Carbon nanofibers were synthetized as follows: a polymer solution (PS) was prepared by dissolving 612 mg of polyacrylonitrile (PAN, P.M. 150,000 g mol^{-1}) and 88.4 mg of polymethylmethacrylate (PMMA, P.M. 350,000 g mol^{-1}) in 10 ml of N, N-dimethylformamide (DFM, 98.80%). The PS was stirred for 18 h and transferred to a glass syringe of the electrospinning system. The synthesis conditions were as follows: 15 cm of distance between the syringe´s needle and the aluminium collector, a voltage of 15 kV and a flow rate of 0.7 ml h^{-1}. Afterward, polymeric nanofibers (PNFs) were stabilized at 250°C for 3 h in air and then carbonized at 700°C under a nitrogen (N_2) atmosphere for 3 h with a heat step of 5°C min^{-1}.

The ternary composite was obtained by chemical bath deposition (CBD) technique using the CNFS as substrate. First, 0.605 g of $SnCl_2*2H_2O$ and 602 g of $SbCl_3$ were dissolved in a solution of HCl and ethanol (1:4 v/v). After, 30 ml of 1M tartaric acid, 25 ml of 0.5 M thioacetamide and 20 ml of distilled water were added. The pH was adjusted to 8 with an ammonium hydroxide solution. Then, the CNFs were immersed into the bath solution at 80°C during 4 h. Finally, the $Sn_xSb_yS_z$ /CNFs were recovered and subject to thermal treatment at 300 °C for 1 h in N_2 atmosphere at heat step of 10°C min^{-1}. This nanocomposite was labelled as $Sn_xSb_yS_z/CNFs_{300}$.

2.2 Physicochemical characterization

Morphology and elemental chemical composition were analyzed with a scanning electron microscope PHILIPS XL 30 ESEM (SEM) coupled with an EDAX Oxford X-act detector. Crystalline structure was determined with a Bruker D8Advance diffractometer (CuKα, λ= 1.54056 Å) in a 2θ range of 10 to 70°. The elemental chemical surface states were determined by X-ray photoelectron spectroscopy with an XPS-Thermo Scientific K-Alpha$^+$. Fourier-transform infrared (FTIR) spectra were acquired using a Perkin Elmer Spectrum Frontier spectrometer (4000-500 cm^{-1}).

2.3 Electrochemical measurements

The working electrodes were fabricated as follows: a mixture of composite, carbon black (Vulcan XC72) and alginic acid sodium salt (weight ratio 3:6:1) was homogeneously dispersed in deionized water. The high amount of carbon used for the electrodes was to avoid limitations in the electronic transport to the active material; as this is a preliminary work, it was envision to learn about the properties of the active material and not to produce a commercial battery. Then, the dispersion was deposited on the copper foil (diameter = 18 mm) and dried at 75 °C for 12 h. The composite mass loading was of 1.2 mg/cm^2.

Electrochemical measurements were performed in a El-CELL (ECC-AIR), which was assembled in an Ar-filled glove box. Metallic sodium and fiberglass were used as counter electrode and separator, respectively. A solution of 0.005 M $NaCl_4$ dissolved in propylene carbonate was used as electrolyte. Cyclic voltammetry (CV) curves were obtained at scan rate of 0.08 mV s^{-1} in a potential range of 2.50 to 0.02 V vs Na/Na^+ in a BioLogic VSP-300 potentiostat. Electrochemical impedance spectroscopy (EIS) measurements were carried out in a frequency range of 500 kHz to 200 mHz with an AC amplitude of 50 mV. The charge/discharge curves were measured using a BST8-MA battery testing system in a potential range of 0.08 to 2.50 V.

3. RESULTS AND DISCUSSION

3.1 Structural characterization

Figure 1 shows the X-ray patterns of CNFs, $Sn_xSb_yS_z$/CNFs and $Sn_xSb_yS_z$/CNFs$_{300}$. The CNFs pattern shows a broad peak at ≈ 2θ= 24.8°, which correspond to the amorphous carbon phase. Moreover, $Sn_xSb_yS_z$/CNFs shows three diffraction peaks at 2θ= 32.12, 39.43 and 51.86°, which corresponding to the (040), (041), and (151) planes, respectively, which can be assigned to the herzenbergite (SnS, PDF# 39-0354). Two peaks of lower intensity at 2θ= 16° and 24° corresponding to the (200) and (101) planes, respectively of Stibnite (Sb_2S_3-PDF#42-1393) were also identified. The foregoing corroborates that the $Sn_xSb_yS_z$/CNFs contains binary phases of the chalcogenides SnS and Sb_2S_3; as expected, usually Sb_2S_3 synthetized by CBD technique is very stable [13].

Moreover, the diffraction pattern of $Sn_xSb_yS_z$/CNFs$_{300}$ shows peaks at 2θ= 23.77, 25.20, 28.79, and 50.32° corresponding to the (101), (221), (501), and (1082) planes, respectively, assigned to the $SnSb_2S_4$ [14], this ternary compound is formed between 200 and 879 °C [15,17]. Additionally, some peaks of binary compounds such as SnS and Sb_2S_3 were also detected. These results are in good agreement with the reported by C. Chen et al. [12], who also obtained a ternary chalcogenide and binary phases/ CNFs composites when annealed at 350°C.

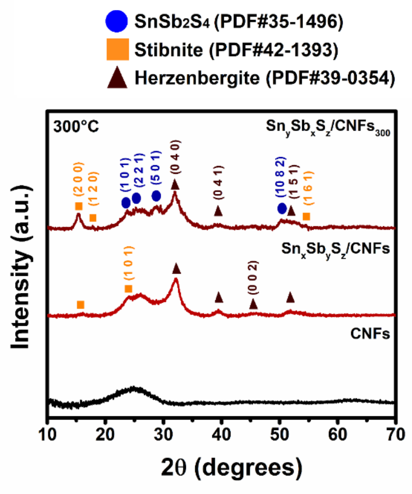

Figure 1. XRD patterns of CNFs, $Sn_xSb_yS_z$/CNF composites before and after thermal treatment at 300°C.

3.2 Morphology and elemental composition

Figure 2a shows the SEM micrograph of the PNFs, which have a morphology like a "prayer beads" with a wide diameter distribution (0.30 to 1.20 µm). The bead formation can be attributed to undissolved polymer in PS. Furthermore, after the carbonization process the CNFs show diameters in a range of 20 to 130 nm, while the beads diameter decreased to approximately 400 nm.

After the CBD process, the surface of CNFs is covered with spherical particles of SnS and Sb_2S_3 with a size of 1.0 to 2.5 µm (Figure 2c). As expected, spherical morphology of SnS and Sb_2S_3 is commonly obtained due to the presence of Sn^{2+} and Sb^{3+} ions with S^{2-} in the chemical bath solution [14,16,18]. Additionally, the elemental composition determined by EDS of $Sn_xSb_yS_z$/CNFs is of 82.55, 4.22, 4.96, and 8.27 at. % of C, Sb, Sn and S, respectively.

On the other hand, the $Sn_xSb_yS_z/CNFs_{300}$ shows changes in its microstructure due to the formation of the ternary $SnSb_2S_4$ on the surface of CNFs (Figure 2d). Besides, the particle size of the chalcogenides is in the range of 0.40 to 3.00 µm, and the elemental composition of the composite is of 91.26 at. % C, 1.31 at. % Sb, 1.70 at. % Sn, 2.07 at. % O and 3.44 at. % S. The presence of oxygen would be associated with the partial oxidation of the ternary material.

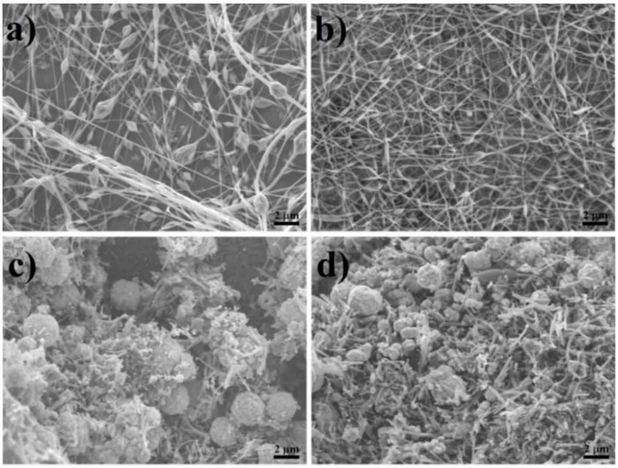

Figure 2. SEM micrographs of (a) PNFs, (b) CNFs, and $Sn_xSb_yS_z$/CNFs composite (c) prior thermal treatment (d) treated at 300°C.

The FTIR spectra of CNFs and $Sn_xSb_yS_z/CNFs_{300}$ are shown in figure 3. Absorption bands are observed at 2920, 2659, and 2324 cm^{-1} which corresponding to the –COOH functional groups. Meanwhile, the bands at 1995 cm^{-1}, 1883 cm^{-1}, 1575-1237 cm^{-1}, 1144 cm^{-1}, and 668 cm^{-1} are assigned to the C=O bond, C≡N bond, C=C bond, C-N bond, and C=C bond, respectively, which are contained in the structure of the CNFs [17,19,20].

Moreover, $Sn_xSb_yS_z/CNFs_{300}$ shows three absorption bands at 892, 596, and 553 cm^{-1} are associated with Sn-S, S-Sb-S and O-Sb-O bons, respectively [21-23], which confirms the formation of SnS and Sb_2S_3 compounds in good agreement with XRD results

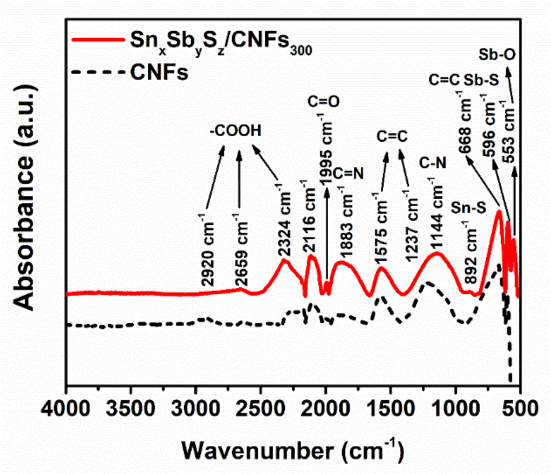

Figure 3. FTIR spectra of the CNFs and $Sn_xSb_yS_z$/CNFs

Figure 4a shows the XPS survey spectra of $Sn_xSb_yS_z$/$CNFs_{300}$, which shows signals corresponding to Sn 3d, Sb 3d, S 2p, O 1s, N 1s, and C 1s. The high-resolution of C 1s region (Figure 4b) shows deconvoluted peaks at 285.03, 285.83, 287.23, and 288.93 eV assigned to C-C, C-N, C≡N, and C=O, respectively. These species can be formed during the carbonization process of the PAN and PMMA polymers used as precursors to obtain CNFs. Meanwhile, the high-resolution of N 1s region shows three peaks at 398.43, 400.03, and 401.13 eV corresponding to N-pyridinic (N1), N-pyrrolic (N2), and N-graphic (N3) nitrogen species, respectively (Figure 4c). It has been reported that the presence of N_1 and N_3 in carbon-based materials can improve the capacity of Na^+ storage [24].

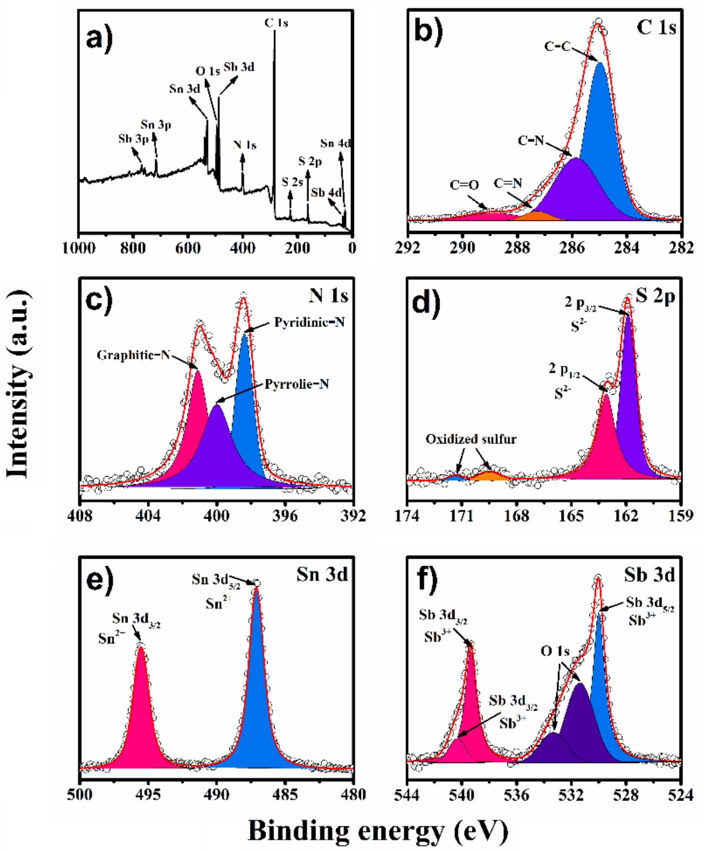

Figure 4. (a) XPS survey spectrum and high-resolution spectra of C 1s (b) and N 1s (c) S 2p (d), Sn 3d (e), and Sn 3d (e) of Sn$_x$Sb$_y$S$_z$/CNFs.

Regarding to the chalcogenides, the high-resolution spectra of S 2p, Sn 3d and Sb 3d peaks are shown in figures 4d, 4e, and 4f, respectively. The peaks at 161.93 and 163.03 eV are attributed to S 2p$_{3/2}$ and S 2p$_{1/2}$, respectively, which is associated to S^{2-}, while the peaks at 169.53 and 171.33 eV corresponding to oxidized sulphur species (Figure 4d) [25]. Moreover, the two strong peaks observed at 487.13 and 495.53 eV (Figure 4e), are assigned to Sn 3d$_{5/2}$ and Sn 3d$_{3/2}$, respectively, which is in good agreement with the Sn^{2+} oxidation state of SnS and SnSb$_2$S$_4$ detected by XRD.

On another hand, the high-resolution Sb 3d region shows peaks corresponding to Sb 3d$_{5/2}$ at 530.0 eV, and a doublet from the spin-orbit of Sb 3d$_{3/2}$ (539.3, and 540.3 eV); additionally, two peaks corresponding to O 1s has been detected (531.3 and 533.3 eV). The high-intense peaks at 530.0 and 539.3 eV correspond to Sb^{3+} in Sb$_2$S$_3$ and SnSb$_2$S$_4$ [26]. Moreover, the low-intensity peak 540.33 eV can be attributed at Sb^{3+} in Sb$_2$O$_3$ [27]. Therefore, the XPS results confirm that Sn$_x$Sb$_y$S$_z$ is formed on the surface of

CNFs, in addition to secondary phases such as SnS and Sb_2S_3 in the ternary compound, as it is discussed in the XRD sections

3.3 Electrochemical performance

Figure 5 shows cyclic voltammetry (CV) curves during the first three cycles of operation. As can be seen, CNFs show a reduction peak at about 2.2 V during the first cycle (Figure 5a) which is associated with the formation of the solid electrolyte interphase (SEI) and decreases in the subsequent cycles [24]. In addition, there a pronounced broad reduction peak at about 0.4 V (Figure 5b) related to the Na^+ intercalation (sodiation process) into CNFs [24,28]; while, the desodiation of Na^+ from CNFs confirmed by a peak at 0.8 V [12].

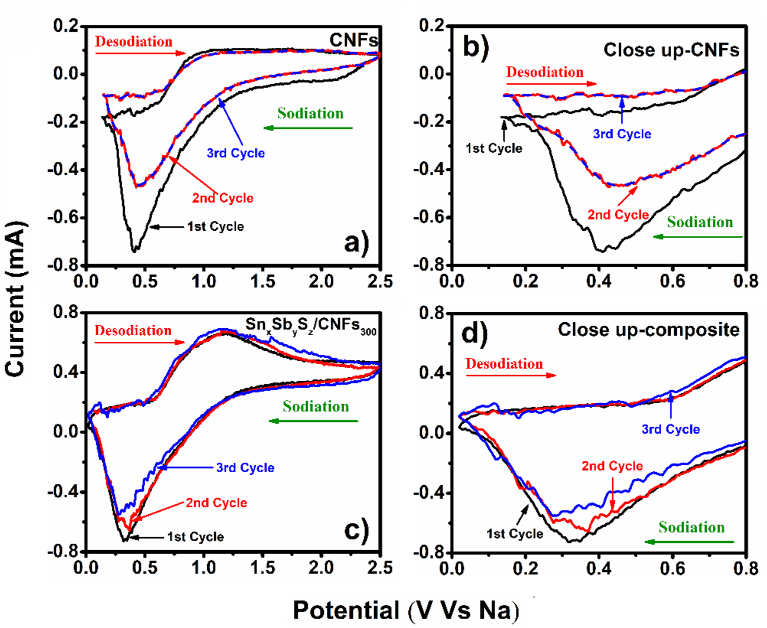

Figure 5. Cyclic voltammetry curves of CNFs (a) and close up CNFs (b); $Sn_xSb_yS_z$/CNFs (c) and close up $Sn_xSb_yS_z$/CNFs (d) at a scan rate of 0.08 mV s^{-1} in the potential range of 0.02-2.5V vs Na.

On the other hand, $Sn_xSb_yS_z/CNFs_{300}$ composite (Figure 5c), shows a broad peak at the potential range of 1.00 to 0.02 V during the first cycle, which is attributed to the combined processes of conversion and alloying reactions of the chalcogenides species (SnS, Sb_2S_3, and $SnSb_2S_4$) and the intercalation of Na^+ ions in the CNFs. Meanwhile, a broad oxidation peak can be seen at the potential range of 0.55 to 1.5 V corresponding to the desodiation process of the Na-Sn, Na-Sb, and Na-S alloys and the re-formation of SnS, Sb_2S_3, $SnSb_2S_4$ phases [26,27], besides the de-intercalation of Na^+ from the CNFs. It is not possible to separate between the processes occurring in the different materials; however, given the shape of the voltammograms of the CNFs with and without sulphides, one can infer that the Na^+ storage is dominated by the CNFs. The potentials of the peaks just shift slightly.

The coversion reactions of Na^+ with the different chalcogenide phases are showed in equations (1), (2) and (3) [9,11,26]:

$$SnS + 2Na^+ + 2e^- \leftrightarrow Sn + Na_2S \qquad (1)$$

$$Sb_2S_3 + 6Na^+ + 6e^- \leftrightarrow 2Sb + 3Na_2S \qquad (2)$$

$$SnSb_2S_4 + 8Na^+ + 8e^- \leftrightarrow Sn + 2Sb + 4Na_2S \qquad (3)$$

The charge-discharge cycles were carried out at a current density of 34 mA g^{-1}. Figure 6 shows the charge capacity and effiencincy at different number cycles of the CNFs and $Sn_xSb_yS_z$/CNFs$_{300}$ (weight ratio 1:3). After nine cycles, the charge capacity value is 160.43 mAh g^{-1}, with a coulombic efficiency of 61.40%. The low coulombic efficiency could be due to the high potential limit taken for the desodiation process. Some current is not produced by desodiation, but by processes like electrolyte decomposition. In this regard, the decrease in the discharge capacity of $Sn_xSb_yS_z$/CNFs can be caused by sodiation-induced volume expansion. Besides, the CNFs capacity is 67.91 mAh g^{-1} (charge) with a coulombic efficiency of 18.50% during the first cycle. After nine cycles, the charge capacity is 126.16 mAh g^{-1} with a coulombic efficiency of 34.26%. As can be seen, the reversible capacity of $Sn_xSb_yS_z$/CNFs is higher than the CNFs due to the high theoretical capacity of Sn (847 mAh g^{-1}) and Sb (670 mAh g^{-1}) in comparison with the theoretical capacity of carbonaceous materials (350 mAh g^{-1}). In addition, greater stability is obtained and the transfer of charge towards the CNFs is improved [9, 11].

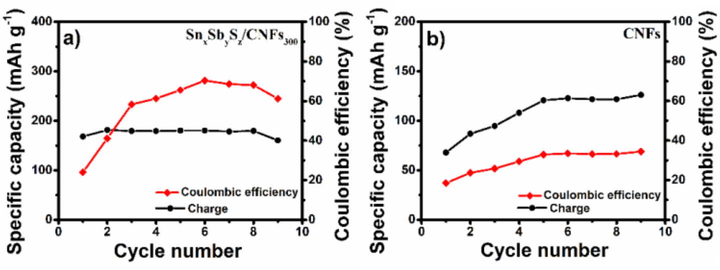

Figure 6. The charge capacity and coulombic efficiency of the of (a) $Sn_xSb_yS_z$/CNFs and (b) CNFs.

The electrochemical impedance spectroscopy (EIS) was implemented for the study and modeling of equivalent circuits (Figure 7), which represents charge transfer kinetics of the CNFss and $Sn_xSb_yS_z$/CNFs. As shown in Figure 7, Nyquist plots of the CNFs and $Sn_xSb_yS_z$/CNFs composite exhibited a semicircle in the high-frequency region (electrochemical doble layer and charge transfer reaction) [29]. Furthermore, an equivalent circuit has been obtained (insert: Figure 7), which is composed of R_S, contacts resistance; Q_{SEI}, constant phase element due to the electrolyte; R_{ELE} , electrode-electrolyte interface resistance; Q_{ct}, constant phase element of Na^+, and R_{ct} (charge transfer resistance of Na^+) [25,30]. The R_{ct} of the composite is 78.64 Ω, while for the CNFs R_{ct} = 115.03 Ω.

This result indicates that the incorporation of chalcogenide on the CNFs improve the Na^+ ion transfer [12,26, 31].

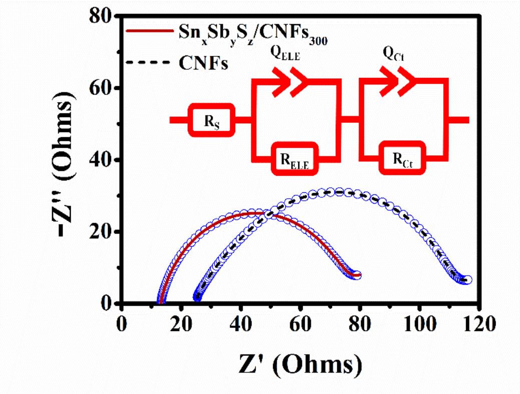

Figure 7. Nyquist plot of the CNFs and $Sn_xSb_yS_z$/CNFs.

4. CONCLUSION

A $Sn_xSb_yS_z$/CNFs composite was obtained by CBD and electrospinning techniques. The physicochemical characterization shows the formation of $SnSb_2S_4$ ternary with additional phases of SnS and Sb_2S_3 after thermal treatment at 300°C. It can be found that the CNFs surface was totally covered by spherical particles with sizes of 0.40 to 3.00 µm, which were attributed to the incorporation of the metal chalcogenides phases (SnS, Sb_2S_3, and $SnSb_2S_4$. Their presence promotes different storage mechanisms of Na^+ such as conversion reaction, alloying and intercalation. In this regard, the composite has high capacity due to the conversion and alloying reactions of Na^+ with the SnS, Sb_2S_3, and $SnSb_2S_4$ compounds. This study represents a preliminary result demonstrating that the addition of the sulfides to the CNFs increase their capacity and charge transfer characteristics.

ACKNOWLEDGEMENTS

The authors acknowledge M.C. Sergio Rodríguez-Arias, Dr. Martha Elena Rivas-Aguilar, M.Sc. Maria del Socorro Garcia-Guillermo, and Dr. Raquel Garza-Hernández from CINVESTAV-Saltillo for their technical support in the measurements of XRD, SEM, UV-Vis, and XPS analyses. This work was financially supported by CONACYT through the grants CB2015-250632 and CB2016-286160.

REFERENCES

[1] P.K. Nayak, L. Yang, W. Brehm, and P. Adelhelm, *Chem. Int. Ed.* **57**, 102-120 (2018).
[2] J.Y. Hwang, S.T. Myung, and Y.K. Sun, *Chem. Soc. Rev*. **46**, 3529-3614 (2017).
[3] M.S. Balogun, Y.L. Qiu, P. Liu, and Y. Tong, *Carbon* **98**, 162-178 (2016).
[4] Y. You, and A. Manthiram, *Adv. Energy. Mater. Int.* **8**, 1-12 (2018).
[5] J. Deng, W.B. Luo, S.L. Chou, H.K. Liu, and S.X. Dou, *Adv. Energy. Mater.* **8**, 1-17 (2018).
[6] T. Jin, Q. Han, Y. Wang, and L. Jiao, *Small* **14**, 1-26 (2018).
[7] H. Hou, X. Qui, W. Wei, Y. Zhang, and X. Ji, *Adv. Energy. Mater.* **7**, 1-30 (2017).
[8] M. Lao, Y. Zhang, W. Luo, Q. Yan W. Sun, And S.X. Dou, *Adv. Mater.* **29**, 1-23 (2017).
[9] Y. Zhang, Q. Zhou, J. Zhu, Q. Yan, S.X Dou, and W. Sun, *Funct. Mater.* **27**, 1-34 (2017).
[10] Y. Liang, W.H. Lai, Z. Miao, and S.L. Chou, *Nano Energy* **14**, 1-20 (2018).
[11] J.M. Jung, C.L. Lee, S. Yu, and I.D. Kim, *Nano Lett.* **4**, 703-750 (2016).
[12] C. Chen, G. Li, J. Zhu, Y. Lu, M. Jiang, Y. Hu, Z. Shen, and X. Zhang, *Carbon* **120**, 380-391 (2017).
[13] P.K. Nair, A.R. García-Angelmo, and M.T.S. Nair, *Phys. Status. Solidi A.* **213**, 170-177 (2016).
[14] L.A. Rodríguez-Guadarrama, I.L. Alonso-Lemus, J. Campos-Álvarez, And J. Escorcia-García, *MRS. Adv.* **4**, 2035-2042 (2019).
[15] U. Chalapachi, B. Poornaprakash, and S.H. Park, J. Sol. Energy. 139, 238-248 (2016).
[16] H. Dittrich, A. Stadler, D. Topa, H.J. Schimper, and A. Basch, *Phys. Status Solidi A* **206**, 1034-1041 (2009).
[17] D. Abdelkader, F.C. Akkari, N. Khemiri, R. Miloua, F. Antoni, B. Gallas, and M. Kanzari, *Physica B: Condensed Matter.* **546**, 33-43 (2018).
[18] U. Chalapachi, B. Poornaprakash, C.H. Ahn, and S.H. Park, *Mater. Sci. Semicond. Process.* **84**, 138-143 (2018).
[19] W. Leang, and B. Pan, *Forest* **10**, 1-12 (2019).
[20] M. Keskinates, B. Yilmaz, Y. Ulusu, and M. Bayrakci, *Mater. Chem. Phys.* **205**, 522-529 (2018).
[21] D.A. Gopakumar, A.R. Pai, Y.B. Pottathara, D. Pasquini, L.C. Morais, M. Luke, N. Kalarikkal, y. Grohens, and S. Thomas, *Appl. Mater. Interfaces.* **23**, 20032-20043 (2018).
[22] V.R. Minna Reddy, S. Gedi, C. Park, and R.W. Miles, *Curr. Appl. Phys.* **15**, 588-598 (2015).
[23] S. Aksaya, T. Özer, and M. Zor, *Eur. Phys. J. Appl. Phys.* **47**, p1-p3 (2009).
[24] M. Muneeb, B. Ismail, T. Fazal, R.A. Khan, A.M. Khan, A. Bilal, B. Muhammad, and A.R. Khan, *Arab. J. Chem.* **4**, 1117-1125 (2018).
[25] J. Xia, K. Jiang, J. Xie, S. Gou, L. Liu, Y. Zhang, S. Nie, Y. Yuan, H. Yan, and X. Wang, *Chem. Eng. J.* **359**, 1244-1251 (2019).
[26] H. Zhai, H. Jiang, Y. Qian, X. Cai, H. Liu, Y. Qiu, M. Jin, F. Xiu, X. Liu, and L. Lai, *Mater. Chem. Phys.* **240**, 1-8 (2020).
[27] Y. Wu, P. Nie, L. Wu, H. Dou, and X. Zhang, *Chem. Eng. J.* **334**, 932-938 (2018).
[28] C.J. Diliegros-Godines, J. Santos-Cruz, N.R. Mathews, And M. Pal, *J. Mater. Sci.* **53**, 11562-11573 (2018).
[29] C. Zou, L. Zhang, X. Hu, Z. Wang, T. Wik, And M. Peacht, *J. Power Sources* **30**, 286-296 (2018).
[30] M. Kakunuri, S. Kaushik, A. Saini, and C.S. Sharma, *Bull. Mater. Sci.* **3,** 435-439 (2017).
[31] X. Yan, Z. Tai, J. Chen, And Q. Xue, *Nanoscale* **3**, 212-216 (2011).